Edinburgh Research Explorer

Calculation of the hadronic vacuum polarization contribution to the muon anomalous magnetic moment

Calculation of the hadronic vacuum polarization contribution to the muon anomalous magnetic moment

T. Blum,[1] P.A. Boyle,[2] V. Gülpers,[3] T. Izubuchi,[4,5] L. Jin,[1,5]
C. Jung,[4] A. Jüttner,[3] C. Lehner,[4,∗] A. Portelli,[2] and J.T. Tsang[2]

(RBC and UKQCD Collaborations)

[1]*Physics Department, University of Connecticut, Storrs, CT 06269-3046, USA*
[2]*School of Physics and Astronomy, The University of Edinburgh, Edinburgh EH9 3FD, UK*
[3]*School of Physics and Astronomy, University of Southampton, Southampton SO17 1BJ, UK*
[4]*Physics Department, Brookhaven National Laboratory, Upton, NY 11973, USA*
[5]*RIKEN-BNL Research Center, Brookhaven National Laboratory, Upton, NY 11973, USA*
(Dated: January 22, 2018)

We present a first-principles lattice QCD+QED calculation at physical pion mass of the leading-order hadronic vacuum polarization contribution to the muon anomalous magnetic moment. The total contribution of up, down, strange, and charm quarks including QED and strong isospin breaking effects is found to be $a_\mu^{\mathrm{HVP\ LO}} = 715.4(16.3)(9.2) \times 10^{-10}$, where the first error is statistical and the second is systematic. By supplementing lattice data for very short and long distances with experimental R-ratio data using the compilation of Ref. [1], we significantly improve the precision of our calculation and find $a_\mu^{\mathrm{HVP\ LO}} = 692.5(1.4)(0.5)(0.7)(2.1) \times 10^{-10}$ with lattice statistical, lattice systematic, R-ratio statistical, and R-ratio systematic errors given separately. This is the currently most precise determination of the leading-order hadronic vacuum polarization contribution to the muon anomalous magnetic moment. In addition, we present the first lattice calculation of the light-quark QED correction at physical pion mass.

INTRODUCTION

The anomalous magnetic moment of the muon a_μ is defined as the deviation of the Landé factor g_μ from Dirac's relativistic quantum mechanics result, $a_\mu = \frac{g_\mu - 2}{2}$. It is one of the most precisely determined quantities in particle physics and is currently known both experimentally (BNL E821) [2] and from a standard model theory calculation [3] to approximately $1/2$ parts per million.

Interestingly, the standard model result a_μ^{SM} deviates from the experimental measurement a_μ^{EXP} at the 3–4 sigma level, depending on which determination of the leading-order hadronic vacuum polarization $a_\mu^{\mathrm{HVP\ LO}}$ is used. One finds

$$a_\mu^{\mathrm{EXP}} - a_\mu^{\mathrm{SM}} = 25.0(4.3)(2.6)(6.3) \times 10^{-10}\ [4]\,,$$
$$31.8(4.1)(2.6)(6.3) \times 10^{-10}\ [5]\,,$$
$$26.8(3.4)(2.6)(6.3) \times 10^{-10}\ [6]\,, \quad (1)$$

where the quoted errors correspond to the uncertainty in $a_\mu^{\mathrm{HVP\ LO}}$, $a_\mu^{\mathrm{SM}} - a_\mu^{\mathrm{HVP\ LO}}$, and a_μ^{EXP}. This tension may hint at new physics beyond the standard model of particle physics such that a reduction of uncertainties in Eq. (1) is highly desirable. New experiments at Fermilab (E989) [7] and J-PARC (E34) [8] intend to decrease the experimental uncertainty by a factor of four. First results of the E989 experiment may be available before the end of 2018 [9] such that a reduction in uncertainty of the $a_\mu^{\mathrm{HVP\ LO}}$ contribution is of timely interest.

In the following, we perform a complete first-principles calculation of $a_\mu^{\mathrm{HVP\ LO}}$ in lattice QCD+QED at physical pion mass with non-degenerate up and down quark masses and present results for the up, down, strange, and charm quark contributions. Our lattice calculation of the light-quark QED correction to $a_\mu^{\mathrm{HVP\ LO}}$ is the first such calculation performed at physical pion mass. In addition, we replace lattice data at very short and long distances by experimental $e^+ e^-$ scattering data using the compilation of Ref. [1], which allows us to produce the currently most precise determination of $a_\mu^{\mathrm{HVP\ LO}}$.

COMPUTATIONAL METHOD

The general setup of our non-perturbative lattice computation is described in Ref. [10]. We compute

$$a_\mu = 4\alpha^2 \int_0^\infty dq^2 f(q^2)[\Pi(q^2) - \Pi(q^2 = 0)]\,, \quad (2)$$

where $f(q^2)$ is a known analytic function [10] and $\Pi(q^2)$ is defined as $\sum_x e^{iqx}\langle J_\mu(x)J_\nu(0)\rangle = (\delta_{\mu\nu}q^2 - q_\mu q_\nu)\Pi(q^2)$ with sum over space-time coordinate x and $J_\mu(x) = i\sum_f Q_f \overline{\Psi}_f(x)\gamma_\mu\Psi_f(x)$. The sum is over up, down, strange, and charm quark flavors with QED charges $Q_{\mathrm{up,\ charm}} = 2/3$ and $Q_{\mathrm{down,\ strange}} = -1/3$. For convenience we do not explicitly write the superscript HVP LO. We compute $\Pi(q^2)$ using the kernel function of Refs. [11, 12]

$$\Pi(q^2) - \Pi(q^2 = 0) = \sum_t \left(\frac{\cos(qt) - 1}{q^2} + \frac{1}{2}t^2 \right) C(t) \quad (3)$$

with $C(t) = \frac{1}{3}\sum_{\vec{x}}\sum_{j=0,1,2}\langle J_j(\vec{x},t)J_j(0)\rangle$. With appropriate definition of w_t, we can therefore write

$$a_\mu = \sum_t w_t C(t).\qquad(4)$$

The correlator $C(t)$ is computed in lattice QCD+QED with dynamical up, down, and strange quarks and non-degenerate up and down quark masses. We compute the missing contributions to a_μ from bottom quarks and from charm sea quarks in perturbative QCD [13] by integrating the time-like region above 2 GeV and find them to be smaller than 0.3×10^{-10}.

We tune the bare up, down, and strange quark masses $m_{\rm up}$, $m_{\rm down}$, and $m_{\rm strange}$ such that the π^0, π^+, K^0, and K^+ meson masses computed in our calculation agree with the respective experimental measurements [14]. The lattice spacing is determined by setting the Ω^- mass to its experimental value. We perform the calculation as a perturbation around an isospin-symmetric lattice QCD computation [15, 16] with two degenerate light quarks with mass $m_{\rm light}$ and a heavy quark with mass $m_{\rm heavy}$ tuned to produce a pion mass of 135.0 MeV and a kaon mass of 495.7 MeV [17]. The correlator is expanded in the fine-structure constant α as well as $\Delta m_{\rm up,\,down} = m_{\rm up,\,down} - m_{\rm light}$, and $\Delta m_{\rm strange} = m_{\rm strange} - m_{\rm heavy}$. We write

$$C(t) = C^{(0)}(t) + \alpha C^{(1)}_{\rm QED}(t) + \sum_f \Delta m_f C^{(1)}_{\Delta m_f}(t)$$
$$+ \mathcal{O}(\alpha^2, \alpha\Delta m, \Delta m^2),\qquad(5)$$

where $C^{(0)}(t)$ is obtained in the lattice QCD calculation at the isospin symmetric point and the expansion terms define the QED and strong isospin-breaking (SIB) corrections, respectively. We keep only the leading corrections in α and Δm_f which is sufficient for the desired precision.

We insert the photon-quark vertices perturbatively with photons coupled to local lattice vector currents multiplied by the renormalization factor Z_V [17]. We use $Z_A \approx Z_V$ for the charm [22] and QED corrections. The SIB correction is computed by inserting scalar operators in the respective quark lines. The procedure used for effective masses in such a perturbative expansion is explained in Ref. [18]. We use the finite-volume QED$_{\rm L}$ prescription [19] and remove the universal $1/L$ and $1/L^2$ corrections to the masses [20] with spatial lattice size L. The effect of $1/L^3$ corrections is small compared to our statistical uncertainties. We find $\Delta m_{\rm up} = -0.00050(1)$, $\Delta m_{\rm down} = 0.00050(1)$, and $\Delta m_{\rm strange} = -0.0002(2)$ for the 48I lattice ensemble described in Ref. [17]. The shift of the Ω^- mass due to the QED correction is significantly smaller than the lattice spacing uncertainty and its effect on $C(t)$ is therefore not included separately.

Figure 1 shows the quark-connected and quark-disconnected contributions to $C^{(0)}$. Similarly, Fig. 2 shows the relevant diagrams for the QED correction to
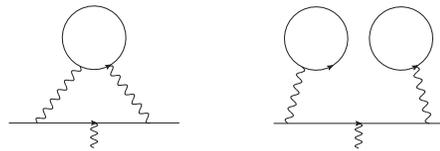

FIG. 1. Quark-connected (left) and quark-disconnected (right) diagram for the calculation of $a_\mu^{\rm HVP\ LO}$. We do not draw gluons but consider each diagram to represent all orders in QCD.
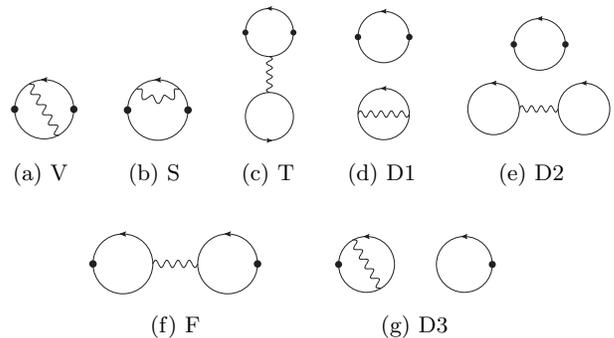

FIG. 2. QED-correction diagrams with external pseudo-scalar or vector operators.

the meson spectrum and the hadronic vacuum polarization. The external vertices are pseudo-scalar operators for the former and vector operators for the latter. We refer to diagrams S and V as the QED-connected and to diagram F as the QED-disconnected contribution. We note that only the parts of diagram F with additional gluons exchanged between the two quark loops contribute to $a_\mu^{\rm HVP\ LO}$ as otherwise an internal cut through a single photon line is possible. For this reason, we subtract the separate quantum-averages of quark loops in diagram F. In the current calculation, we neglect diagrams T, D1, D2, and D3. This approximation is estimated to yield an $\mathcal{O}(10\%)$ correction for isospin splittings [21] for which the neglected diagrams are both SU(3) and $1/N_c$ suppressed. For the hadronic vacuum polarization the contribution of neglected diagrams is still $1/N_c$ suppressed and we adopt a corresponding 30% uncertainty.

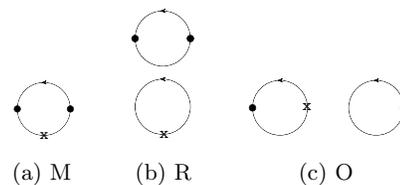In Fig. 3, we show the SIB diagrams. In the calcu-

FIG. 3. Strong isospin-breaking correction diagrams. The crosses denote the insertion of a scalar operator.
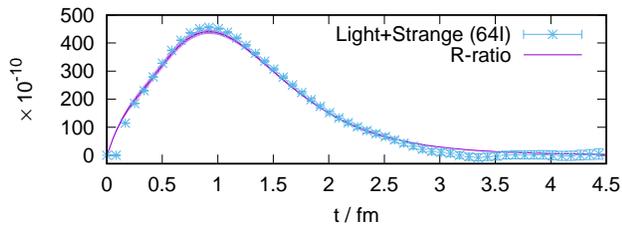
FIG. 4. Comparison of $w_t C(t)$ obtained using R-ratio data [1] and lattice data on our 64I ensemble.

lation presented here, we only include diagram M. For the meson masses this corresponds to neglecting the sea quark mass correction, which we have previously [17] determined to be an $\mathcal{O}(2\%)$ and $\mathcal{O}(14\%)$ effect for the pions and kaons, respectively. This estimate is based on the analytic fits of (H7) and (H9) of Ref. [17] with ratios $C_2^{m_\pi,\ \kappa}/C_1^{m_\pi,\ \kappa}$ given in Tab. XVII of the same reference. For the hadronic vacuum polarization the contribution of diagram R is negligible since $\Delta m_{\mathrm{up}} \approx -\Delta m_{\mathrm{down}}$ and diagram O is SU(3) and $1/N_c$ suppressed. We therefore assign a corresponding 10% uncertainty to the SIB correction.

We also compute the $\mathcal{O}(\alpha)$ correction to the vector current renormalization factor Z_V used in $C^{(0)}$ [17, 18] and find a small correction of approximately 0.05% for the light quarks.

We perform the calculation of $C^{(0)}$ on the 48I and 64I ensembles described in Ref. [17] for the up, down, and strange quark-connected contributions. For the charm contribution we also perform a global fit using additional ensembles described in Ref. [22]. The quark-disconnected contribution as well as QED and SIB corrections are computed only on ensemble 48I.

For the noisy light quark connected contribution, we employ a multi-step approximation scheme with low-mode averaging [23] over the entire volume and two levels of approximations in a truncated deflated solver (AMA) [24–27] of randomly positioned point sources. The low-mode space is generated using a new Lanczos method working on multiple grids [28]. Our improved statistical estimator for the quark disconnected diagrams is described in Ref. [29] and our strategy for the strange quark is published in Ref. [30]. For diagram F, we re-use point-source propagators generated in Ref. [31].

The correlator $C(t)$ is related to the R-ratio data [11] by $C(t) = \frac{1}{12\pi^2} \int_0^\infty d(\sqrt{s})R(s)se^{-\sqrt{s}t}$ with $R(s) = \frac{3s}{4\pi\alpha^2}\sigma(s, e^+e^- \to \mathrm{had})$. In Fig. 4 we compare a lattice and R-ratio evaluation of $w_t C(t)$ and note that the R-ratio data is most precise at very short and long distances, while the lattice data is most precise at intermediate distances. We are therefore led to also investigate a position-space "window method" [11, 32] and write

$$a_\mu = a_\mu^{\mathrm{SD}} + a_\mu^{\mathrm{W}} + a_\mu^{\mathrm{LD}} \tag{6}$$

with $a_\mu^{\mathrm{SD}} = \sum_t C(t)w_t[1 - \Theta(t, t_0, \Delta)]$, $a_\mu^{\mathrm{W}} = \sum_t C(t)w_t[\Theta(t, t_0, \Delta) - \Theta(t, t_1, \Delta)]$, and $a_\mu^{\mathrm{LD}} = \sum_t C(t)w_t\Theta(t, t_1, \Delta)$, where each contribution is accessible from both lattice and R-ratio data. We define $\Theta(t, t', \Delta) = [1 + \tanh[(t - t')/\Delta]]/2$ which we find to be helpful to control the effect of discretization errors by the smearing parameter Δ. We then take a_μ^{SD} and a_μ^{LD} from the R-ratio data and a_μ^{W} from the lattice. In this work we use $\Delta = 0.15$ fm, which we find to provide a sufficiently sharp transition without increasing discretization errors noticeably. This method takes the most precise regions of both datasets and therefore may be a promising alternative to the proposal of Ref. [33].

ANALYSIS AND RESULTS

In Tab. I we show our results for the individual as well as summed contributions to a_μ for the window method as well as a pure lattice determination. We quote statistical uncertainties for the lattice data (S) and the R-ratio data (RST) separately. For the quark-connected up, down, and strange contributions, the computation is performed on two ensembles with inverse lattice spacing $a^{-1} = 1.730(4)$ GeV (48I) as well as $a^{-1} = 2.359(7)$ GeV (64I) and a continuum limit is taken. The discretization error (C) is estimated by taking the maximum of the squared measured $\mathcal{O}(a^2)$ correction as well as a simple $(a\Lambda)^4$ estimate, where we take $\Lambda = 400$ MeV. We find the results on the 48I ensemble to differ only a few percent from the continuum limit. This holds for the full lattice contribution as well as the window contributions considered in this work. For the quark-connected charm contribution additional ensembles described in Ref. [22] are used and the maximum of the above and a $(am_c)^4$ estimate is taken as discretization error. The remaining contributions are small and only computed on the 48I ensemble for which we take $(a\Lambda)^2$ as estimate of discretization errors.

For the up and down quark-connected and disconnected contributions, we correct finite-volume effects to leading order in finite-volume position-space chiral perturbation theory [34]. Note that in our previous publication of the quark-disconnected contribution [29], we added this finite-volume correction as an uncertainty but did not shift the central value. We take the largest ratio of p^6 to p^4 corrections of Tab. 1 of Ref. [35] as systematic error estimate of neglected finite-volume errors (V). For the SIB correction we also include the sizeable difference of the corresponding finite and infinite-volume chiral perturbation theory calculation as finite-volume uncertainty. For the QED correction, we repeat the computation using an infinite-volume photon (QED$_\infty$ [36]) and include the difference to the QED$_{\mathrm{L}}$ result as a finite-volume error. Further details of the QED$_\infty$ procedure are provided as supplementary material.

$a_\mu^{ud,\,conn,\,isospin}$	$202.9(1.4)_S(0.2)_C(0.1)_V(0.2)_A(0.2)_Z$	$649.7(14.2)_S(2.8)_C(3.7)_V(1.5)_A(0.4)_Z(0.1)_{E48}(0.1)_{E64}$
$a_\mu^{s,\,conn,\,isospin}$	$27.0(0.2)_S(0.0)_C(0.1)_A(0.0)_Z$	$53.2(0.4)_S(0.0)_C(0.3)_A(0.0)_Z$
$a_\mu^{c,\,conn,\,isospin}$	$3.0(0.0)_S(0.1)_C(0.0)_Z(0.0)_M$	$14.3(0.0)_S(0.7)_C(0.1)_Z(0.0)_M$
$a_\mu^{uds,\,disc,\,isospin}$	$-1.0(0.1)_S(0.0)_C(0.0)_V(0.0)_A(0.0)_Z$	$-11.2(3.3)_S(0.4)_V(2.3)_L$
$a_\mu^{QED,\,conn}$	$0.2(0.2)_S(0.0)_C(0.0)_V(0.0)_A(0.0)_Z(0.0)_E$	$5.9(5.7)_S(0.3)_C(1.2)_V(0.0)_A(0.0)_Z(1.1)_E$
$a_\mu^{QED,\,disc}$	$-0.2(0.1)_S(0.0)_C(0.0)_V(0.0)_A(0.0)_Z(0.0)_E$	$-6.9(2.1)_S(0.4)_C(1.4)_V(0.0)_A(0.0)_Z(1.3)_E$
a_μ^{SIB}	$0.1(0.2)_S(0.0)_C(0.2)_V(0.0)_A(0.0)_Z(0.0)_{E48}$	$10.6(4.3)_S(0.6)_C(6.6)_V(0.1)_A(0.0)_Z(1.3)_{E48}$
$a_\mu^{udsc,\,isospin}$	$231.9(1.4)_S(0.2)_C(0.1)_V(0.3)_A(0.2)_Z(0.0)_M$	$705.9(14.6)_S(2.9)_C(3.7)_V(1.8)_A(0.4)_Z(2.3)_L(0.1)_{E48}$ $(0.1)_{E64}(0.0)_M$
$a_\mu^{QED,\,SIB}$	$0.1(0.3)_S(0.0)_C(0.2)_V(0.0)_A(0.0)_Z(0.0)_E(0.0)_{E48}$	$9.5(7.4)_S(0.7)_C(6.9)_V(0.1)_A(0.0)_Z(1.7)_E(1.3)_{E48}$
$a_\mu^{R-ratio}$	$460.4(0.7)_{RST}(2.1)_{RSY}$	
a_μ	$692.5(1.4)_S(0.2)_C(0.2)_V(0.3)_A(0.2)_Z(0.0)_E(0.0)_{E48}$ $(0.0)_b(0.1)_c(0.0)_{\overline{S}}(0.0)_{\overline{Q}}(0.0)_M(0.7)_{RST}(2.1)_{RSY}$	$715.4(16.3)_S(3.0)_C(7.8)_V(1.9)_A(0.4)_Z(1.7)_E(2.3)_L$ $(1.5)_{E48}(0.1)_{E64}(0.3)_b(0.2)_c(1.1)_{\overline{S}}(0.3)_{\overline{Q}}(0.0)_M$

TABLE I. Individual and summed contributions to a_μ multiplied by 10^{10}. The left column lists results for the window method with $t_0 = 0.4$ fm and $t_1 = 1$ fm. The right column shows results for the pure first-principles lattice calculation. The respective uncertainties are defined in the main text.

We furthermore propagate uncertainties of the lattice spacing (A) and the renormalization factors Z_V (Z). For the quark-disconnected contribution we adopt the additional long-distance error discussed in Ref. [29] (L) and for the charm contribution we propagate uncertainties from the global fit procedure [22] (M). Systematic errors of the R-ratio computation are taken from Ref. [1] and quoted as (RSY). The neglected bottom quark (b) and charm sea quark (c) contributions as well as effects of neglected QED ($\overline{Q}$) and SIB ($\overline{S}$) diagrams are estimated as described in the previous section.

For the QED and SIB corrections, we assume dominance of the low-lying $\pi\pi$ and $\pi\gamma$ states and fit $C_{QED}^{(1)}(t)$ as well as $C_{\Delta m_f}^{(1)}(t)$ to $(c_1 + c_0 t)e^{-Et}$, where we vary c_0 and c_1 for fixed energy E. The resulting p-values are larger than 0.2 for all cases and we use this functional form to compute the respective contribution to a_μ. For the QED correction, we vary the energy E between the lowest $\pi\pi$ and $\pi\gamma$ energies and quote the difference as additional uncertainty (E). For the SIB correction, we take E to be the $\pi\pi$ ground-state energy.

For the light quark contribution of our pure lattice result we use a bounding method [37] similar to Ref. [38] and find that upper and lower bounds meet within errors at $t = 3.0$ fm. We vary the ground-state energy that enters this method [39] between the free-field and interacting value [40]. For the 48I ensemble we find $E_0^{free} = 527.3$ MeV, $E_0 = 517.4$ MeV $+ \mathcal{O}(1/L^6)$ and for the 64I ensemble we have $E_0^{free} = 536.1$ MeV, $E_0 = 525.1$ MeV $+ \mathcal{O}(1/L^6)$. We quote the respective uncertainties as (E48) and (E64). The variation of $\pi\pi$ ground-state energy on the 48I ensemble also enters the SIB correction as described above.

Figure 5 shows our results for the window method with $t_0 = 0.4$ fm. While the partial lattice and R-ratio contributions change by several 100×10^{-10}, the sum changes only at the level of quoted uncertainties. This provides a non-trivial consistency check between the lattice and
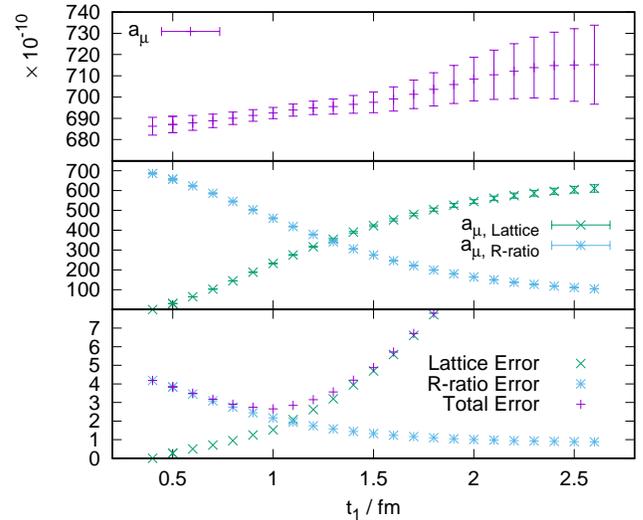
FIG. 5. We show results for the window method with $t_0 = 0.4$ fm as a function of t_1. The top panel shows the combined a_μ, the middle panel shows the partial contributions of the lattice and R-ratio data, and the bottom shows the respective uncertainties.

the R-ratio data for length scales between 0.4 fm and 2.6 fm. We expand on this check in the supplementary material. The uncertainty of the current analysis is minimal for $t_1 = 1$ fm, which we take as our main result for the window method. For $t_0 = t_1$ we reproduce the value of Ref. [1]. In Fig. 6, we show the t_1-dependence of individual lattice contributions and compare our results with previously published results in Fig. 7. Our combined lattice and R-ratio result is more precise than the R-ratio computation by itself and reduces the tension to the other R-ratio results. Results for different window parameters t_0 and t_1 and a comparison of individual components with previously published results are provided as supplementary material.

FIG. 6. The individual lattice components of the window method with $t_0 = 0.4$ fm as function of t_1.

FIG. 7. Our results (RBC/UKQCD 2018) compared to previously published results. The green data-points are pure lattice computations, the orange data-point is our combined window analysis, and the purple data-points are pure R-ratio results. The references are ETMC 2013 [41], HPQCD 2016 [42], Mainz 2017 [43], BMW 2017 [39], HLMNT 2011 [4], DHMZ 2012 [44], DHMZ 2017 [6], Jegerlehner 2017 [5], and No new physics [3]. The innermost error-bar corresponds to the statistical uncertainty.

CONCLUSION

We have presented both a complete first-principles calculation of the leading-order hadronic vacuum polarization contribution to the muon anomalous magnetic moment from lattice QCD+QED at physical pion mass as well as a combination with R-ratio data. For the former we find $a_\mu^{\text{HVP LO}} = 715.4(16.3)(9.2) \times 10^{-10}$, where the first error is statistical and the second is systematic. For the latter we find $a_\mu^{\text{HVP LO}} = 692.5(1.4)(0.5)(0.7)(2.1) \times 10^{-10}$ with lattice statistical, lattice systematic, R-ratio statistical, and R-ratio systematic errors given separately. This is the currently most precise determination of $a_\mu^{\text{HVP LO}}$ corresponding to a 3.7σ tension

$$a_\mu^{\text{EXP}} - a_\mu^{\text{SM}} = 27.4(2.7)(2.6)(6.3) \times 10^{-10}. \quad (7)$$

The presented combination of lattice and R-ratio data also serves to provide additional non-trivial cross-checks between lattice and R-ratio data. The precision of this computation will be improved in future work including simulations at smaller lattice spacings and at larger volumes.

DiRAC is part of the National E-Infrastructure. The software used includes BAGEL (GNU GPLv2 license), CPS, GPT, Grid (GNU GPLv2 license), and LatAnalyze (GNU GPLv3 license).

————————

* Corresponding author; clehner@quark.phy.bnl.gov
[1] F. Jegerlehner, "alphaQEDc17," (2017).
[2] G. Bennett *et al.* (Muon G-2), Phys.Rev. **D73**, 072003 (2006), arXiv:hep-ex/0602035 [hep-ex].
[3] C. Patrignani *et al.* (Particle Data Group), Chin. Phys. C **40**, 100001 (2016), including the 2017 update for the 2016 edition at http://pdg.lbl.gov.
[4] K. Hagiwara, R. Liao, A. D. Martin, D. Nomura, and T. Teubner, J.Phys. **G38**, 085003 (2011), arXiv:1105.3149 [hep-ph].
[5] F. Jegerlehner, (2017), arXiv:1705.00263 [hep-ph].
[6] M. Davier, A. Hoecker, B. Malaescu, and Z. Zhang, Eur. Phys. J. **C77**, 827 (2017), arXiv:1706.09436 [hep-ph].
[7] R. Carey, K. Lynch, J. Miller, B. Roberts, W. Morse, *et al.*, "The New (g-2) Experiment: A proposal to measure the muon anomalous magnetic moment to +-0.14 ppm precision," (2009).
[8] M. Aoki *et al.*, KEK-J-PARC **PAC2009**, 12 (2009).
[9] Private communication with the Fermilab E989 collaboration.
[10] T. Blum, Phys.Rev.Lett. **91**, 052001 (2003), arXiv:hep-lat/0212018 [hep-lat].
[11] D. Bernecker and H. B. Meyer, Eur. Phys. J. **A47**, 148 (2011), arXiv:1107.4388 [hep-lat].
[12] X. Feng, S. Hashimoto, G. Hotzel, K. Jansen, M. Petschlies, *et al.*, Phys.Rev. **D88**, 034505 (2013), arXiv:1305.5878 [hep-lat].
[13] R. V. Harlander and M. Steinhauser, Comput. Phys. Commun. **153**, 244 (2003), arXiv:hep-ph/0212294 [hep-ph].
[14] We minimize the sum of squared differences of computed and measured meson masses.
[15] G. M. de Divitiis *et al.*, JHEP **04**, 124 (2012), arXiv:1110.6294 [hep-lat].
[16] G. M. de Divitiis, R. Frezzotti, V. Lubicz, G. Martinelli, R. Petronzio, G. C. Rossi, F. Sanfilippo, S. Simula, and N. Tantalo (RM123), Phys. Rev. **D87**, 114505 (2013), arXiv:1303.4896 [hep-lat].
[17] T. Blum *et al.* (RBC, UKQCD), Phys. Rev. **D93**, 074505 (2016), arXiv:1411.7017 [hep-lat].
[18] P. Boyle, V. Gülpers, J. Harrison, A. Jüttner, C. Lehner, A. Portelli, and C. T. Sachrajda, JHEP **09**, 153 (2017), arXiv:1706.05293 [hep-lat].
[19] M. Hayakawa and S. Uno, Prog. Theor. Phys. **120**, 413 (2008), arXiv:0804.2044 [hep-ph].
[20] S. Borsanyi *et al.*, Science **347**, 1452 (2015), arXiv:1406.4088 [hep-lat].
[21] S. Borsanyi *et al.* (Budapest-Marseille-Wuppertal), Phys. Rev. Lett. **111**, 252001 (2013), arXiv:1306.2287 [hep-lat].
[22] P. A. Boyle, L. Del Debbio, A. Jüttner, A. Khamseh, F. Sanfilippo, and J. T. Tsang, JHEP **12**, 008 (2017), arXiv:1701.02644 [hep-lat].
[23] T. A. DeGrand and S. Schäfer, *Lattice field theory. Proceedings, 22nd International Symposium, Lattice 2004, Batavia, USA, June 21-26, 2004*, Nucl. Phys. Proc. Suppl. **140**, 296 (2005), [,296(2004)], arXiv:hep-lat/0409056 [hep-lat].
[24] S. Collins, G. Bali, and A. Schäfer, *Proceedings, 25th International Symposium on Lattice field theory (Lattice 2007): Regensburg, Germany, July 30-August 4, 2007*, PoS **LATTICE2007**, 141 (2007), arXiv:0709.3217 [hep-lat].
[25] G. S. Bali, S. Collins, and A. Schäfer, Comput. Phys. Commun. **181**, 1570 (2010), arXiv:0910.3970 [hep-lat].
[26] T. Blum, T. Izubuchi, and E. Shintani, Phys. Rev. **D88**, 094503 (2013), arXiv:1208.4349 [hep-lat].
[27] E. Shintani, R. Arthur, T. Blum, T. Izubuchi, C. Jung, and C. Lehner, Phys. Rev. **D91**, 114511 (2015), arXiv:1402.0244 [hep-lat].
[28] M. A. Clark, C. Jung, and C. Lehner, in *35th International Symposium on Lattice Field Theory (Lattice 2017) Granada, Spain, June 18-24, 2017* (2017) arXiv:1710.06884 [hep-lat].
[29] T. Blum, P. A. Boyle, T. Izubuchi, L. Jin, A. Jüttner, C. Lehner, K. Maltman, M. Marinkovic, A. Portelli, and M. Spraggs, Phys. Rev. Lett. **116**, 232002 (2016), arXiv:1512.09054 [hep-lat].
[30] T. Blum *et al.* (RBC/UKQCD), JHEP **04**, 063 (2016), [Erratum: JHEP05,034(2017)], arXiv:1602.01767 [hep-lat].
[31] T. Blum, N. Christ, M. Hayakawa, T. Izubuchi, L. Jin, C. Jung, and C. Lehner, Phys. Rev. Lett. **118**, 022005 (2017), arXiv:1610.04603 [hep-lat].
[32] C. Lehner (RBC, UKQCD), in *35th International Symposium on Lattice Field Theory (Lattice 2017) Granada, Spain, June 18-24, 2017* (2017) arXiv:1710.06874 [hep-lat].
[33] J. Charles, D. Greynat, and E. de Rafael, (2017), arXiv:1712.02202 [hep-ph].
[34] C. Aubin, T. Blum, P. Chau, M. Golterman, S. Peris, and C. Tu, Phys. Rev. **D93**, 054508 (2016), arXiv:1512.07555 [hep-lat].
[35] J. Bijnens and J. Relefors, JHEP **12**, 114 (2017), arXiv:1710.04479 [hep-lat].
[36] C. Lehner and T. Izubuchi, *Proceedings, 32nd International Symposium on Lattice Field Theory (Lattice 2014)*, PoS **LATTICE2014**, 164 (2015), arXiv:1503.04395 [hep-lat].
[37] C. Lehner, "The hadronic vacuum polarization contribution to the muon anomalous magnetic moment," (2016), RBRC Workshop on Lattice Gauge Theories.
[38] S. Borsanyi, Z. Fodor, T. Kawanai, S. Krieg, L. Lellouch, R. Malak, K. Miura, K. K. Szabo, C. Torrero, and B. Toth, Phys. Rev. **D96**, 074507 (2017), arXiv:1612.02364 [hep-lat].
[39] S. Borsanyi *et al.* (Budapest-Marseille-Wuppertal), (2017), arXiv:1711.04980 [hep-lat].
[40] M. Lüscher, Commun. Math. Phys. **105**, 153 (1986).
[41] F. Burger, X. Feng, G. Hotzel, K. Jansen, M. Petschlies, and D. B. Renner (ETM), JHEP **02**, 099 (2014), arXiv:1308.4327 [hep-lat].
[42] B. Chakraborty, C. T. H. Davies, P. G. de Oliviera, J. Koponen, G. P. Lepage, and R. S. Van de Water, Phys. Rev. **D96**, 034516 (2017), arXiv:1601.03071 [hep-lat].
[43] M. Della Morte, A. Francis, V. Gülpers, G. Herdoíza, G. von Hippel, H. Horch, B. Jäger, H. B. Meyer, A. Nyffeler, and H. Wittig, JHEP **10**, 020 (2017), arXiv:1705.01775 [hep-lat].

[44] M. Davier, A. Hoecker, B. Malaescu, and Z. Zhang, Eur. Phys. J. **C71**, 1515 (2011), [Erratum: Eur. Phys. J.C72,1874(2012)], arXiv:1010.4180 [hep-ph].

[45] D. Giusti, V. Lubicz, G. Martinelli, F. Sanfilippo, and S. Simula, JHEP **10**, 157 (2017), arXiv:1707.03019 [hep-lat].

[46] B. Chakraborty *et al.* (Fermilab Lattice, LATTICE-HPQCD, MILC), (2017), arXiv:1710.11212 [hep-lat].

[47] V. Gülpers, A. Francis, B. Jäger, H. Meyer, G. von Hippel, and H. Wittig, *Proceedings, 32nd International Symposium on Lattice Field Theory (Lattice 2014)*, PoS **LATTICE2014**, 128 (2014), arXiv:1411.7592 [hep-lat].

SUPPLEMENTARY MATERIAL

In this section we expand on a selection of technical details and add results to facilitate cross-checks of different calculations of $a_\mu^{\rm HVP\ LO}$.

Continuum limit: The continuum limit of a selection of light-quark window contributions a_μ^W is shown in Fig. 8. We note that the results on the coarse lattice differ from the continuum limit only at the level of a few percent. We attribute this mild continuum limit to the favorable properties of the domain-wall discretization used in this work. This is in contrast to a rather steep continuum extrapolation that occurs using staggered quarks as seen, e.g., in Ref. [42].

The mild continuum limit for light quark contributions is consistent with a naive power-counting estimate of $(a\Lambda)^2 = 0.05$ with $\Lambda = 400$ MeV and suggests that remaining discretization errors may be small. Since we find such a mild behavior not just for a single quantity but for all studied values of a_μ^W with t_0 ranging from 0.3 fm to 0.5 fm and t_1 ranging from 0.3 fm to 2.6 fm, we suggest that it is rather unlikely that the mild behavior is result of an accidental cancellation of higher-order terms in an expansion in a^2. This lends support to our quoted discretization error based on an $\mathcal{O}(a^4)$ estimate. In future work, this will be subject to further scrutiny by adding a data-point at an additional lattice spacing.

Energy re-weighting: The top panel of Fig. 9 shows the weighted correlator $w_t C(t)$ for the full a_μ as well as short-distance and long-distance projections $a_\mu^{\rm SD}$ and $a_\mu^{\rm LD}$ for $t_0 = 0.4$ fm and $t_1 = 1.5$ fm. The bottom panel of Fig. 9 shows the corresponding contributions to a_μ separated by energy scale $\sqrt{s}$. We notice that, as expected, $a_\mu^{\rm SD}$ has reduced contributions from low-energy scales and $a_\mu^{\rm LD}$ has reduced contributions from high-energy scales. In the limit of projection to sufficiently long distances, we
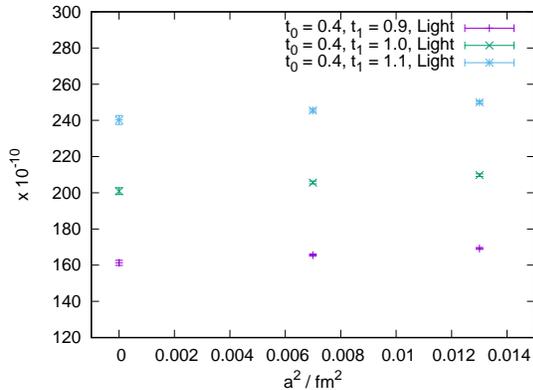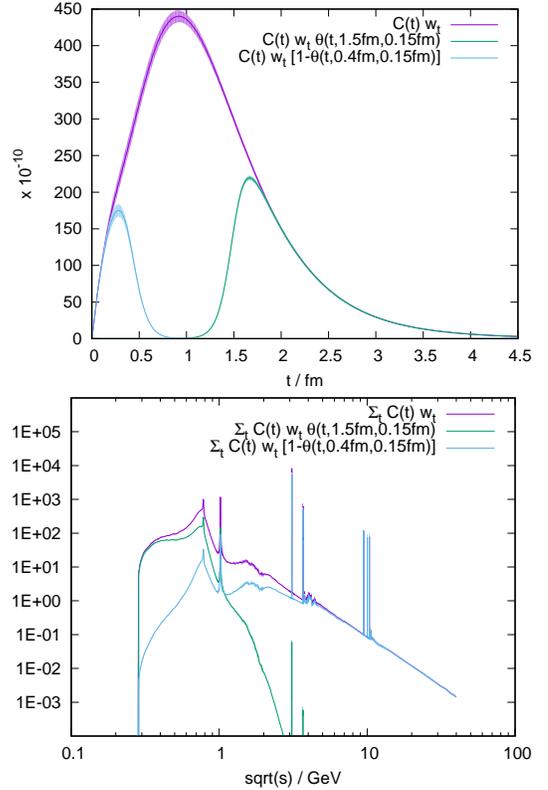

FIG. 9. Window of R-ratio data in Euclidean position space (top) and the effect of the window in terms of re-weighting energy regions (bottom).

may attempt to contrast the R-ratio data directly with an exclusive study of the low-lying $\pi\pi$ states in the lattice calculation. This is left to future work.

Statistics of light-quark contribution: We use an improved statistical estimator including a full low-mode average for the light-quark connected contribution in the isospin symmetric limit as discussed in the main text. For this estimator, we find that we are able to saturate the statistical fluctuations to the gauge noise for 50 point sources per configuration. For the 48I ensemble we measure on 127 gauge configurations and for the 64I ensemble we measure on 160 gauge configurations. Our result is therefore obtained from a total of approximately 14k domain-wall fermion propagator calculations.

Results for other values of t_0 and t_1: In Tabs. S I-S VII we provide results for different choices of window parameters t_0 and t_1. We believe that this additional data may facilitate cross-checks between different lattice collaborations in particular also with regard to the up and down quark connected contribution in the isospin limit.

FIG. 8. Continuum limit of light-quark $a_\mu^{\rm W}$ with $t_0 = 0.4$ fm and $\Delta = 0.15$ fm.

$a_\mu^{ud,\ conn,\ isospin}$	$317.8(2.9)_S(0.2)_C(0.4)_V(0.7)_A(0.3)_Z$
$a_\mu^{s,\ conn,\ isospin}$	$35.9(0.2)_S(0.0)_C(0.2)_A(0.0)_Z$
$a_\mu^{c,\ conn,\ isospin}$	$3.0(0.0)_S(0.1)_C(0.0)_Z(0.0)_M$
$a_\mu^{uds,\ disc,\ isospin}$	$-2.9(0.4)_S(0.1)_C(0.0)_V(0.0)_A(0.0)_Z$
$a_\mu^{QED,\ conn}$	$0.6(0.5)_S(0.0)_C(0.1)_V(0.0)_A(0.0)_Z(0.0)_E$
$a_\mu^{QED,\ disc}$	$-0.6(0.2)_S(0.0)_C(0.1)_V(0.0)_A(0.0)_Z(0.0)_E$
a_μ^{SIB}	$0.7(0.6)_S(0.0)_C(0.5)_V(0.0)_A(0.0)_Z(0.1)_{E48}$
$a_\mu^{udsc,\ isospin}$	$353.9(2.9)_S(0.3)_C(0.4)_V(0.8)_A(0.3)_Z(0.0)_M$
$a_\mu^{QED,\ SIB}$	$0.7(0.8)_S(0.1)_C(0.5)_V(0.0)_A(0.0)_Z(0.0)_E(0.1)_{E48}$
$a_\mu^{R-ratio}$	$340.9(0.5)_{RST}(1.5)_{RSY}$
a_μ	$695.5(3.0)_S(0.3)_C(0.6)_V(0.8)_A(0.3)_Z(0.0)_E(0.0)_M(0.1)_{E48}(0.0)_b(0.1)_c(0.1)_{\overline{S}}(0.0)_{\overline{Q}}(0.5)_{RST}(1.5)_{RSY}$

TABLE S I. Individual and summed contributions to a_μ multiplied by 10^{10} for the window method with $t_0 = 0.4$ fm and $t_1 = 1.3$ fm. The respective uncertainties are defined in the main text.

$a_\mu^{ud,\ conn,\ isospin}$	$413.1(4.9)_S(0.3)_C(0.7)_V(1.3)_A(0.3)_Z$
$a_\mu^{s,\ conn,\ isospin}$	$40.6(0.3)_S(0.0)_C(0.2)_A(0.0)_Z$
$a_\mu^{c,\ conn,\ isospin}$	$3.0(0.0)_S(0.1)_C(0.0)_Z(0.0)_M$
$a_\mu^{uds,\ disc,\ isospin}$	$-5.9(0.7)_S(0.3)_C(0.1)_V(0.0)_A(0.0)_Z$
$a_\mu^{QED,\ conn}$	$1.3(1.0)_S(0.1)_C(0.3)_V(0.0)_A(0.0)_Z(0.1)_E$
$a_\mu^{QED,\ disc}$	$-1.3(0.4)_S(0.1)_C(0.3)_V(0.0)_A(0.0)_Z(0.1)_E$
a_μ^{SIB}	$1.9(1.1)_S(0.1)_C(0.9)_V(0.0)_A(0.0)_Z(0.2)_{E48}$
$a_\mu^{udsc,\ isospin}$	$450.8(5.0)_S(0.5)_C(0.7)_V(1.5)_A(0.4)_Z(0.0)_M$
$a_\mu^{QED,\ SIB}$	$1.8(1.6)_S(0.2)_C(1.0)_V(0.0)_A(0.0)_Z(0.1)_E(0.2)_{E48}$
$a_\mu^{R-ratio}$	$246.5(0.5)_{RST}(1.2)_{RSY}$
a_μ	$699.1(5.2)_S(0.5)_C(1.2)_V(1.5)_A(0.4)_Z(0.1)_E(0.0)_M(0.2)_{E48}(0.0)_b(0.1)_c(0.2)_{\overline{S}}(0.0)_{\overline{Q}}(0.5)_{RST}(1.2)_{RSY}$

TABLE S II. Individual and summed contributions to a_μ multiplied by 10^{10} for the window method with $t_0 = 0.4$ fm and $t_1 = 1.6$ fm. The respective uncertainties are defined in the main text.

$a_\mu^{ud,\ conn,\ isospin}$	$485.7(7.8)_S(0.4)_C(1.1)_V(1.9)_A(0.4)_Z$
$a_\mu^{s,\ conn,\ isospin}$	$42.7(0.4)_S(0.0)_C(0.2)_A(0.0)_Z$
$a_\mu^{c,\ conn,\ isospin}$	$3.0(0.0)_S(0.1)_C(0.0)_Z(0.0)_M$
$a_\mu^{uds,\ disc,\ isospin}$	$-9.1(1.7)_S(0.4)_C(0.1)_V(0.0)_A(0.0)_Z$
$a_\mu^{QED,\ conn}$	$2.0(1.7)_S(0.1)_C(0.4)_V(0.0)_A(0.0)_Z(0.2)_E$
$a_\mu^{QED,\ disc}$	$-2.2(0.6)_S(0.2)_C(0.4)_V(0.0)_A(0.0)_Z(0.2)_E$
a_μ^{SIB}	$3.3(1.7)_S(0.2)_C(1.6)_V(0.0)_A(0.0)_Z(0.3)_{E48}$
$a_\mu^{udsc,\ isospin}$	$522.3(8.0)_S(0.6)_C(1.1)_V(2.1)_A(0.4)_Z(0.0)_M$
$a_\mu^{QED,\ SIB}$	$3.1(2.5)_S(0.3)_C(1.7)_V(0.0)_A(0.0)_Z(0.2)_E(0.3)_{E48}$
$a_\mu^{R-ratio}$	$180.5(0.4)_{RST}(1.0)_{RSY}$
a_μ	$705.9(8.4)_S(0.6)_C(2.0)_V(2.1)_A(0.4)_Z(0.2)_E(0.0)_M(0.3)_{E48}(0.0)_b(0.1)_c(0.3)_{\overline{S}}(0.1)_{\overline{Q}}(0.4)_{RST}(1.0)_{RSY}$

TABLE S III. Individual and summed contributions to a_μ multiplied by 10^{10} for the window method with $t_0 = 0.4$ fm and $t_1 = 1.9$ fm. The respective uncertainties are defined in the main text.

$a_\mu^{ud,\ conn,\ isospin}$	$533.8(11.3)_S(0.4)_C(1.6)_V(2.3)_A(0.4)_Z$
$a_\mu^{s,\ conn,\ isospin}$	$43.5(0.4)_S(0.0)_C(0.3)_A(0.0)_Z$
$a_\mu^{c,\ conn,\ isospin}$	$3.0(0.0)_S(0.1)_C(0.0)_Z(0.0)_M$
$a_\mu^{uds,\ disc,\ isospin}$	$-10.4(3.1)_S(0.5)_C(0.2)_V(0.1)_A(0.0)_Z$
$a_\mu^{QED,\ conn}$	$2.8(2.5)_S(0.2)_C(0.6)_V(0.0)_A(0.0)_Z(0.3)_E$
$a_\mu^{QED,\ disc}$	$-3.2(0.9)_S(0.2)_C(0.6)_V(0.0)_A(0.0)_Z(0.3)_E$
a_μ^{SIB}	$4.9(2.3)_S(0.2)_C(2.3)_V(0.1)_A(0.0)_Z(0.5)_{E48}$
$a_\mu^{udsc,\ isospin}$	$570.0(11.7)_S(0.6)_C(1.6)_V(2.6)_A(0.5)_Z(0.0)_M$
$a_\mu^{QED,\ SIB}$	$4.6(3.6)_S(0.4)_C(2.5)_V(0.1)_A(0.0)_Z(0.4)_E(0.5)_{E48}$
$a_\mu^{R-ratio}$	$137.6(0.4)_{RST}(0.9)_{RSY}$
a_μ	$712.2(12.2)_S(0.8)_C(2.9)_V(2.6)_A(0.4)_Z(0.4)_E(0.0)_M(0.5)_{E48}(0.0)_b(0.1)_c(0.5)_{\overline{S}}(0.1)_{\overline{Q}}(0.4)_{RST}(0.9)_{RSY}$

TABLE S IV. Individual and summed contributions to a_μ multiplied by 10^{10} for the window method with $t_0 = 0.4$ fm and $t_1 = 2.2$ fm. The respective uncertainties are defined in the main text.

$a_\mu^{ud,\ conn,\ isospin}$	$561.6(15.2)_S(0.4)_C(2.0)_V(2.5)_A(0.4)_Z$
$a_\mu^{s,\ conn,\ isospin}$	$43.8(0.4)_S(0.0)_C(0.3)_A(0.0)_Z$
$a_\mu^{c,\ conn,\ isospin}$	$3.0(0.0)_S(0.1)_C(0.0)_Z(0.0)_M$
$a_\mu^{uds,\ disc,\ isospin}$	$-10.1(3.7)_S(0.5)_C(0.2)_V(0.0)_A(0.0)_Z$
$a_\mu^{QED,\ conn}$	$3.6(3.3)_S(0.3)_C(0.7)_V(0.0)_A(0.0)_Z(0.4)_E$
$a_\mu^{QED,\ disc}$	$-4.1(1.2)_S(0.3)_C(0.8)_V(0.0)_A(0.0)_Z(0.5)_E$
a_μ^{SIB}	$6.4(2.9)_S(0.3)_C(3.1)_V(0.1)_A(0.0)_Z(0.7)_{E48}$
$a_\mu^{udsc,\ isospin}$	$598.4(15.7)_S(0.6)_C(2.0)_V(2.8)_A(0.5)_Z(0.0)_M$
$a_\mu^{QED,\ SIB}$	$5.9(4.5)_S(0.5)_C(3.2)_V(0.1)_A(0.0)_Z(0.7)_E(0.7)_{E48}$
$a_\mu^{R-ratio}$	$110.8(0.3)_{RST}(0.8)_{RSY}$
a_μ	$715.1(16.3)_S(0.8)_C(3.8)_V(2.9)_A(0.5)_Z(0.7)_E(0.0)_M(0.7)_{E48}(0.0)_b(0.1)_c(0.6)_{\overline{S}}(0.1)_{\overline{Q}}(0.3)_{RST}(0.8)_{RSY}$

TABLE S V. Individual and summed contributions to a_μ multiplied by 10^{10} for the window method with $t_0 = 0.4$ fm and $t_1 = 2.5$ fm. The respective uncertainties are defined in the main text.

$a_\mu^{ud,\ conn,\ isospin}$	$222.5(1.5)_S(0.2)_C(0.1)_V(0.2)_A(0.2)_Z$
$a_\mu^{s,\ conn,\ isospin}$	$30.5(0.2)_S(0.0)_C(0.1)_A(0.0)_Z$
$a_\mu^{c,\ conn,\ isospin}$	$5.6(0.0)_S(0.3)_C(0.0)_Z(0.0)_M$
$a_\mu^{uds,\ disc,\ isospin}$	$-1.0(0.1)_S(0.0)_C(0.0)_V(0.0)_A(0.0)_Z$
$a_\mu^{QED,\ conn}$	$0.2(0.2)_S(0.0)_C(0.0)_V(0.0)_A(0.0)_Z(0.0)_E$
$a_\mu^{QED,\ disc}$	$-0.2(0.1)_S(0.0)_C(0.0)_V(0.0)_A(0.0)_Z(0.0)_E$
a_μ^{SIB}	$0.1(0.2)_S(0.0)_C(0.2)_V(0.0)_A(0.0)_Z(0.0)_{E48}$
$a_\mu^{udsc,\ isospin}$	$257.6(1.5)_S(0.3)_C(0.2)_V(0.3)_A(0.2)_Z(0.0)_M$
$a_\mu^{QED,\ SIB}$	$0.1(0.3)_S(0.0)_C(0.2)_V(0.0)_A(0.0)_Z(0.0)_E(0.0)_{E48}$
$a_\mu^{R-ratio}$	$436.2(0.6)_{RST}(1.8)_{RSY}$
a_μ	$694.0(1.5)_S(0.3)_C(0.2)_V(0.3)_A(0.2)_Z(0.0)_E(0.0)_M(0.0)_{E48}(0.0)_b(0.1)_c(0.0)_{\overline{S}}(0.0)_{\overline{Q}}(0.6)_{RST}(1.8)_{RSY}$

TABLE S VI. Individual and summed contributions to a_μ multiplied by 10^{10} for the window method with $t_0 = 0.3$ fm and $t_1 = 1$ fm. The respective uncertainties are defined in the main text.

$a_\mu^{ud,\ conn,\ isospin}$	$178.8(1.3)_S(0.1)_C(0.1)_V(0.2)_A(0.2)_Z$
$a_\mu^{s,\ conn,\ isospin}$	$22.8(0.1)_S(0.0)_C(0.1)_A(0.0)_Z$
$a_\mu^{c,\ conn,\ isospin}$	$1.4(0.0)_S(0.1)_C(0.0)_Z(0.0)_M$
$a_\mu^{uds,\ disc,\ isospin}$	$-1.0(0.1)_S(0.0)_C(0.0)_V(0.0)_A(0.0)_Z$
$a_\mu^{QED,\ conn}$	$0.2(0.1)_S(0.0)_C(0.0)_V(0.0)_A(0.0)_Z(0.0)_E$
$a_\mu^{QED,\ disc}$	$-0.2(0.1)_S(0.0)_C(0.0)_V(0.0)_A(0.0)_Z(0.0)_E$
a_μ^{SIB}	$0.1(0.2)_S(0.0)_C(0.2)_V(0.0)_A(0.0)_Z(0.0)_{E48}$
$a_\mu^{udsc,\ isospin}$	$202.0(1.3)_S(0.2)_C(0.1)_V(0.3)_A(0.2)_Z(0.0)_M$
$a_\mu^{QED,\ SIB}$	$0.2(0.3)_S(0.0)_C(0.2)_V(0.0)_A(0.0)_Z(0.0)_E(0.0)_{E48}$
$a_\mu^{R-ratio}$	$489.5(0.7)_{RST}(2.4)_{RSY}$
a_μ	$691.7(1.4)_S(0.2)_C(0.2)_V(0.3)_A(0.2)_Z(0.0)_E(0.0)_M(0.0)_{E48}(0.0)_b(0.1)_c(0.0)_{\overline{S}}(0.0)_{\overline{Q}}(0.7)_{RST}(2.4)_{RSY}$

TABLE S VII. Individual and summed contributions to a_μ multiplied by 10^{10} for the window method with $t_0 = 0.5$ fm and $t_1 = 1$ fm. The respective uncertainties are defined in the main text.
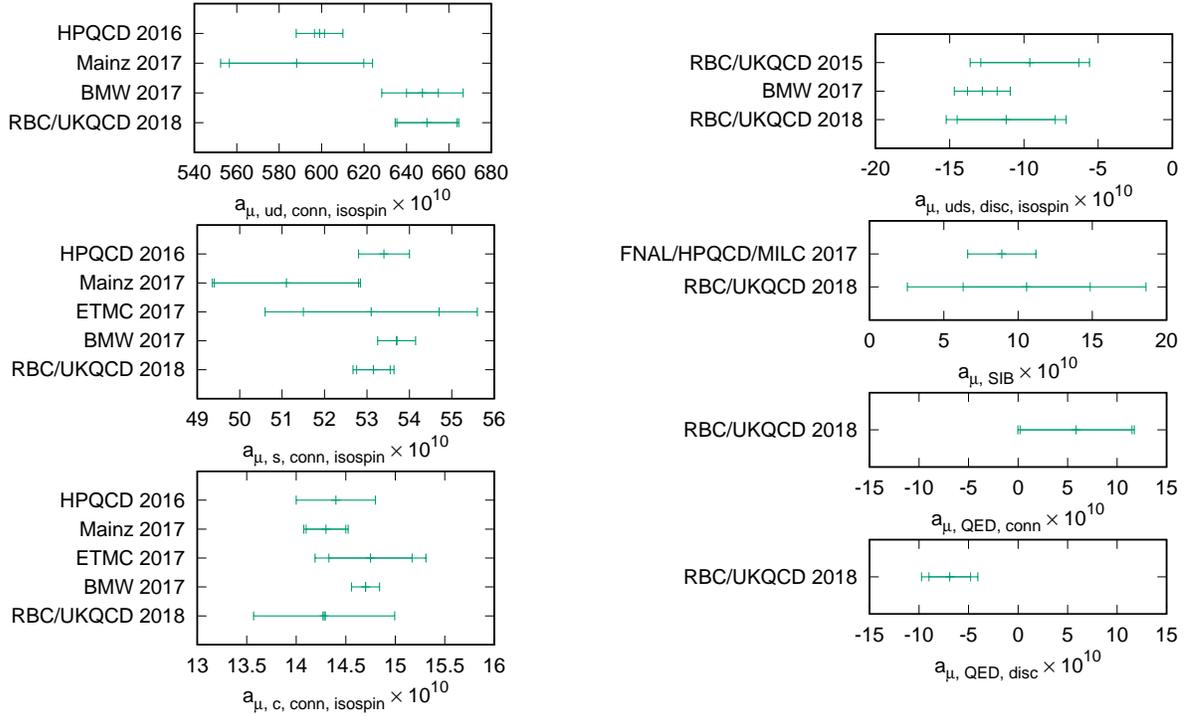
FIG. 10. A comparison of our results with previously published results. The references in order of appearance are HPQCD 2016 [42], Mainz 2017 [43], BMW 2017 [39], ETMC 2017 [45], RBC/UKQCD 2015 [29], and FNAL/HPQCD/MILC 2017 [46]. The innermost error-bar corresponds to the statistical uncertainty.

Comparison of individual contributions: In Fig. 10, we compare our results for individual contributions to $a_\mu^{\text{HVP LO}}$ obtained from a pure lattice QCD+QED calculation to previously published results. We find good agreement between the different lattice computations for all results apart from the up and down quark connected contribution in the isospin limit. Further scrutiny of the tension between the HPQCD 2016 and the BMW 2017 and our RBC/UKQCD 2018 results is desired and will be part of future work. As an additional check we have computed the small QED correction to the strange quark-connected contribution. We find $a_\mu^{\text{s, QED, conn}} = -0.0149(9)_{\text{S}}(8)_{\text{C}}(30)_{\text{V}} \times 10^{-10}$ with error estimates described in the main text. Our result agrees well with $a_\mu^{\text{s, QED, conn}} = -0.018(11) \times 10^{-10}$ of Ref. [45].

Bounding method: As discussed in the main text, we use a bounding method [37] for the light-quark connected contribution in the isospin symmetric limit. In the following we give more details for our method and contrast it with the similar method used in Ref. [38]. Both our method and the method of Ref. [38] build on ideas of Ref. [47].

The correlator $C(t)$ can be written as

$$C(t) = \sum_{n=0}^{N} c_n e^{-E_n t} \tag{S1}$$

with real positive energy levels E_n and the constraint that all $c_n \geq 0$. The correlator

$$\tilde{C}(t; T, \tilde{E}) = \begin{cases} C(t) & t < T, \\ C(T)e^{-(t-T)\tilde{E}} & t \geq T \end{cases} \tag{S2}$$

then defines a strict upper or lower bound of $C(t)$ for each t for an appropriate choice of $\tilde{E}$. For the upper bound, we proceed as Ref. [38] and use the finite-volume ground-state energy E_0 to define

$$C_{\text{upper}}(t) = \tilde{C}(t; T, E_0). \tag{S3}$$

For the lower bound, we use the logarithmic effective mass

$$E_T^* = \log(C(T)/C(T+1)) \tag{S4}$$

and define

$$C_{\text{lower}}(t) = \tilde{C}(t; T, E_T^*) \tag{S5}$$

in contrast to the choice $\tilde{E} \to \infty$ of Ref. [38]. It is straightforward to show that

$$C_{\text{lower}}(t) \leq C(t) \leq C_{\text{upper}}(t) \tag{S6}$$

for all t. This bound is more restrictive compared to the choice of $\tilde{E} \to \infty$. Since the effective mass E_T^* may
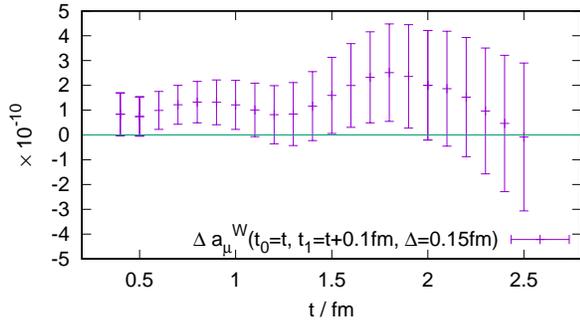
FIG. 11. The difference of window contributions from the lattice and the R-ratio. We show $\Delta a_\mu^W = a_\mu^{W\ \text{Lattice}} - a_\mu^{W\ \text{R-ratio}}$.

become noisy at long distances, we also note that any choice of energy $\tilde{E}$ with $\tilde{E} \geq E_T^*$ provides a strict lower bound.

Consistency of R-ratio and lattice data: In Fig. 11 we show the difference of window contributions $a_\mu^W(t_0, t_1, \Delta)$ from the lattice and the R-ratio with $t_0 = t$, $t_1 = t + 0.1$ fm, and smearing parameter $\Delta = 0.15$ fm. These localized windows are well-defined in the lattice and the R-ratio calculation and allow for a more precise check of consistency at fixed Euclidean time. While we find the lattice calculation to prefer a slightly larger value compared to the R-ratio data of Ref. [1], this difference is statistically not significant. We will reduce the lattice uncertainties in the near future in order to provide a more stringent cross-check between both methods.

As noted in the main text, our result for a combined lattice and R-ratio analysis shown in Fig. 7 is based on the R-ratio compilation used in "Jegerlehner 2017" but is in better agreement with the "HLMNT 2011", "DHMZ 2012", and "DHMZ 2017" results than the pure

"Jegerlehner 2017" result. Our value has replaced over one third of the R-ratio contribution with lattice data and receives its uncertainty in approximate equal parts from lattice and R-ratio data. We are keen on incorporating alternate compilations of data in future studies and to explore the degree to which the lattice analysis can help to understand and reduce tensions between the different compilations.

Estimating QED finite-volume errors: We estimate the finite-volume uncertainty of the hadronic vacuum polarization QED corrections by performing the calculation using an infinite-volume photon (QED$_\infty$) in addition to the QED$_\text{L}$ prescription. We take the difference of both computations as systematic uncertainty due to the finite volume. The procedure for both calculations only differs in the photon propagator that is used. The QED$_\text{L}$ prescription uses the photon propagator

$$G_\text{L}(x) = \frac{1}{V} \sum_k{}' \frac{1}{\hat{k}^2} e^{ikx}, \qquad (S\,7)$$

where $\hat{k}^2 = \sum_\mu 4\sin^2(k_\mu/2)$ and $V = \prod_\mu L_\mu$ with lattice dimensions L_μ. The sum is over all momenta with components $k_\mu = 2\pi n_\mu/L_\mu$ with $n_\mu \in [0, \ldots, L_\mu - 1]$ and the restriction that $k_0^2 + k_1^2 + k_2^2 \neq 0$. For QED$_\infty$ we use instead

$$G_\infty(x) = \int_{-\pi}^\pi \frac{d^4k}{(2\pi)^4} \frac{1}{\hat{k}^2} e^{ikx} \qquad (S\,8)$$

with the constraint

$$-\frac{L_\mu}{2} \leq x_\mu < \frac{L_\mu}{2} \qquad (S\,9)$$

for $\mu \in [0, 1, 2, 3]$.